communications earth & environment

Article

https://doi.org/10.1038/s43247-024-01310-0

Brief and intensive volcanic emissions from Ontong Java Nui heralded Oceanic Anoxic Event 1a

Hironao Matsumoto [1] ✉, Kosuke T. Goto [2], Gen Shimoda [2], Yasuto Watanabe [3,4], Kotaro Shirai [5], Maria Luisa G. Tejada [6], Akira Ishikawa [1,7], Atsushi Ando[8,9], Takashi Sano [10], Junichiro Kuroda[5] & Katsuhiko Suzuki [1]

The volcanic episode that formed Ontong Java Nui (OJN) in the western Pacific ~ 120 million-year-ago is thought to have triggered Oceanic Anoxic Event (OAE) 1a, yet the cause-effect relationship remains insufficiently understood. Here, we present a Pb-Os-C isotope dataset for tracking OJN volcanism across a sedimentary sequence containing OAE1a record in the central Pacific. Lead isotopic evidence strongly supports the deposition of OJN-sourced volcanic ash layers at this site after a paired seawater $\delta^{13}C_{carb}$–$^{187}Os/^{188}Os$ shift and before the onset of OAE1a. The $\delta^{13}C_{carb}$–$^{187}Os/^{188}Os$ shift is attributable to the signature of the initial submarine OJN eruption. The subsequent unradiogenic Pb isotope shifts could represent ash fallout from the brief, explosive subaerial/shallow-marine eruption phase accompanied by intensive volcanic degassing and emissions. The apparent time lag between explosive OJN volcanism and OAE1a is intriguing, which can be accounted for by the delayed increase in the productivity after gas emissions.

Throughout the geologic past, the Earth has experienced recurring pulses of mantle plume volcanism forming large igneous provinces (LIPs). The largest known LIP is the Ontong Java Plateau (OJP), which formed in the western Pacific Ocean during a short period of time in the early Aptian (~Early Cretaceous, 120 Ma) (Fig. 1). Previous studies have revealed that the OJP, Manihiki Plateau (MP), and Hikurangi Plateau (HP) used to form a single enormous complex of oceanic plateaus, now called Ontong Java Nui (OJN)[1,2]. Despite its partial subduction beneath the Solomon Islands[3], the remaining part of OJN still occupies ~1% of Earth's surface today[1]. OJN volcanism has attracted broad interest because of the consistency of its timing with contemporaneous environmental perturbations that certainly caused Oceanic Anoxic Event (OAE) 1a[4] and associated marine biotic crises and evolution[5]. However, because earlier studies linking this early Aptian LIP volcanism to global environmental change relied on spotty radiometric ages from the topmost parts of the OJN, there is appreciable uncertainty in the chronology of OJN activity[6]. Biostratigraphic data from just above the basalt basement at several drill sites suggest that the formation of OJP and the early Aptian environmental crises were almost simultaneous[7,8], although recent ^{40}Ar–^{39}Ar dating suggests much younger radiometric ages for OJP (~117–108 Ma)[9].

Recently, Os and Pb isotopic studies of pelagic sedimentary sections have provided clues to the history of LIP volcanism that are directly integrated with information on palaeoenvironmental changes recorded in the same sequences[4,10]. At the time of OAE1a, Os isotopic data from marine sedimentary sequences have been demonstrated to have shifted sharply, signifying an abrupt influx of mantle-derived Os[4,11]. Coeval Pb isotopic data from silicate fractions ($^{206}Pb/^{204}Pb$, $^{207}Pb/^{204}Pb$, and $^{208}Pb/^{204}Pb$) have been applied as tracers of LIP activity with the capability to differentiate among several basaltic flow types (e.g., Kwaimbaita [kw] /Kroenke [kr]-type basalts and the overlying minor Singgalo [sg]-type basalts on OJP, and high-Ti and

[1]Research Institute for Marine Resources Utilization, Japan Agency for Marine-Earth Science and Technology, 2–15, Natsushima, Yokosuka, Kanagawa 237–0061, Japan. [2]Geological Survey of Japan, AIST, 1-1-1 Higashi, Tsukuba 305-8567, Japan. [3]Department of Earth and Planetary Science, The University of Tokyo, Hongo 7-3-1, Tokyo, Japan. [4]Meteorological Research Institute, Japan Meteorological Agency, 1– 1 Nagamine, Tsukuba, Ibaraki 305-0052, Japan. [5]Atmosphere and Ocean Research Institute, The University of Tokyo, 5-1-5, Kashiwanoha, Kashiwa, Chiba 277-8564, Japan. [6]Research Institute for Marine Geodynamics, Japan Agency for Marine-Earth Science and Technology, 2–15, Natsushima, Yokosuka, Kanagawa 237–0061, Japan. [7]Department of Earth and Planetary Sciences, Tokyo Institute of Technology, 2-12-1 Ookayama, Meguro-ku, Tokyo 152–8550, Japan. [8]Department of Paleobiology, National Museum of Natural History, Smithsonian Institution, Washington, DC, USA. [9]BugWare, Inc., Tallahassee, FL, USA. [10]Department of Geology and Paleontology, National Museum of Nature and Science, Amakubo 1-1-1, Tsukuba, Ibaraki 305-0005, Japan. ✉e-mail: hironao.matsumoto@jamstec.go.jp

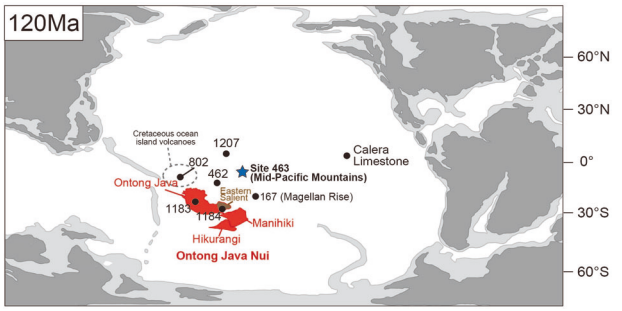

Fig. 1 | Palaeogeographic reconstruction of the Pacific Ocean at 120 Ma[2,5]. The paleo-locations of the Ontong Java Plateau, Manihiki Plateau, and Hikurangi Plateau that comprise the Ontong Java Nui, together with Deep-Sea Drilling Project (DSDP) Site 463 and other DSDP/Ocean Drilling Program (ODP) sites discussed in the text are shown. The dashed circle represents the reconstructed location of the Cretaceous ocean island volcanoes.

low-Ti type basalts on MP)[10]. Although Os isotope studies have successfully established the evolution of seawater Os isotope across OAE1a, which is supported by reproducible results from different ocean basins, the Pb isotopic approach is still uncommon despite its unique potential for detailing the volcanic history of OJN.

At deep-sea drilling project (DSDP) Site 463, a series of borehole cores were recovered from a pelagic carbonate succession in the Mid-Pacific Mountains, ~3000 km to the northeast of OJN (Fig. 1). This deep-sea section contains an exceptionally complete sedimentary record of Pacific OAE1a that has been the subject of a number of multidisciplinary studies[11–13], yet Pb isotopic studies are still critically lacking. In this regard, the lower Aptian sequence at Site 463 is intriguing because it contains tuffaceous sediments. The tuffaceous sediments have previously been inferred to have been derived from volcanic eruptions at OJN[14]; further, potentially correlative volcanic ash layers have been reported from Site 167 (Magellan Rise) and the Calera Limestone (California)[15] (Fig. 1). However, no specific geochemical assessments have been made to identify the provenance of the ash deposits[14,15]. Here, we present a Pb isotope dataset from the Aptian suc-

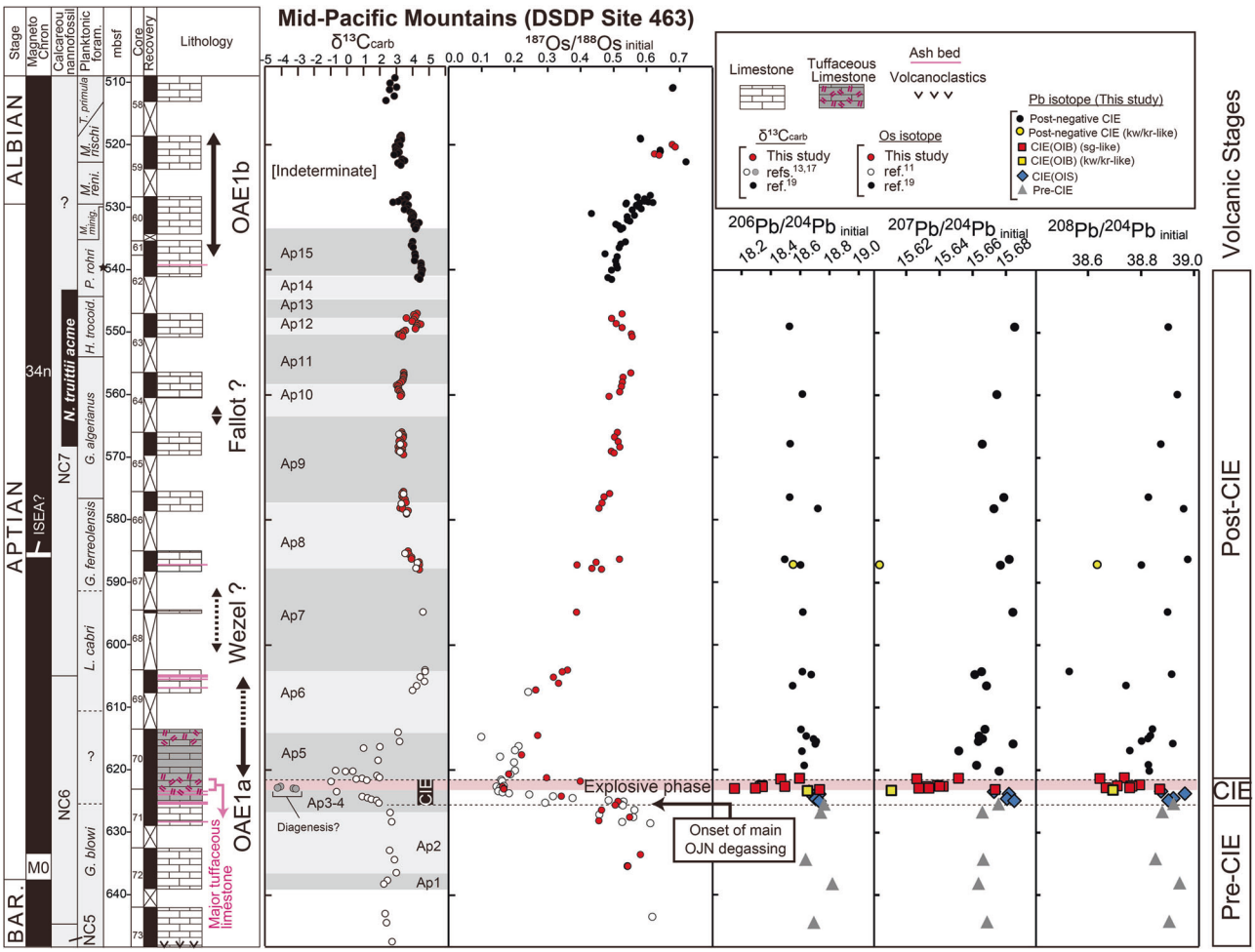

Fig. 2 | New Aptian Pb isotopic profiles of silicate fractions from DSDP site 463 and a compilation of published and new $\delta^{13}C_{carb}$ and Os data. Lithology is based on ref. 16; biostratigraphy is based on refs. 13,19; $\delta^{13}C_{carb}$ data with chemostratigraphic segments (Ap1–Ap15) are based on refs. 13,17,19, and this study; and Os isotopic data are from this study and refs. 11,19. The interval of *Globigerinelloides algerianus* zone is slightly modified based on the newly acquired foraminiferal specimens (Supplementary Fig. S5). Here, according to depth information reported in ref. 16, the basal 10 cm of Core 70 overlaps with the underlying Core 71. To resolve the overlap, we adjusted the previously reported depths of Core 71, Sections 1 and 2 by adding +10 cm. Because there is a 10 cm core gap at the top of Core 71, Section 3, we used the previously reported core depths for the samples from lower than Core 71, Section 2[16]. Abbreviations: mbsf meter, below seafloor, CIE carbon isotope excursion, OAE oceanic anoxic event, OJN Ontong Java Nui, BAR Barremian, kw/kr Kwaimbaita/Kroenke, sg Singgalo, *G. Globigerinelloides*, *L. Leupoldina*, *trocoid. trocoidea*, *P. Paraticinella*, *M. Microhedbergella*, *minig. miniglobularis*, *reni. reni-laevis*, *T. Ticinella*.

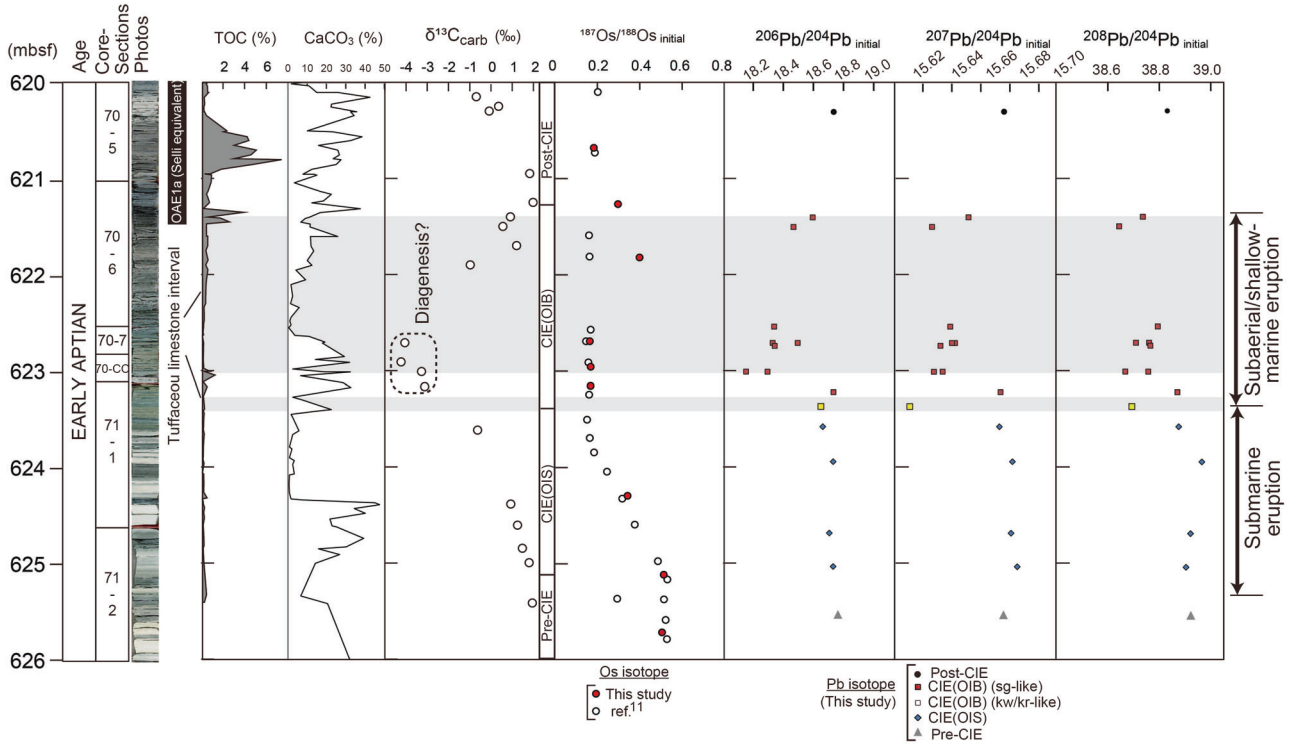

Fig. 3 | Detailed view of the critical lower Aptian interval at DSDP Site 463 (Core 71–Section 2 to Core 70–Section 7). TOC and $CaCO_3$ profiles are compilations of published data by ref. 13. Data for $\delta^{13}C_{carb}$ are from ref. 13; data points enclosed by the dotted line are $\delta^{13}C_{carb}$ values of samples with anomalous Sr isotope ratios affected by selective diagenesis[17]. The Os isotopic data are from ref. 11 and this study and the Pb isotopic data are from this study.

cession at Site 463 that we use, together with updated carbon ($\delta^{13}C_{carb}$) and, Os isotope ($^{187}Os/^{188}Os$) profiles and a biogeochemical model of global carbon (C) and phosphorus (P) cycles, to explore the evolution of OJN volcanism and its causal relationship with OAE1a. We show that the volcanic ash layer just below the organic-rich interval at Site 463 indicates brief but intensive volcanic emissions from OJN prior to the onset of the OAE1a.

Results and discussion

Litho- and chemostratigraphy of DSDP site 463

DSDP Leg 62 recovered a core at Site 463 with a Barremian to Aptian (Lower Cretaceous) sedimentary sequence consisting mostly of limestones and marlstone rich in calcareous microfossils[16] (Fig. 2). As summarized elsewhere[13], a characteristic lower Aptian organic-rich interval (621.45–615.53 meter below seafloor [mbsf], or possibly up to 604.46 mbsf) with total organic carbon (TOC) contents of up to ~8% occurs in the *Globigerinelloides blowi–Leopoldina cabri* planktonic foraminiferal zones, in the NC6 calcareous nannofossil Zone, and 11.9 m above the top-of magnetic Chron M0 (Fig. 2). Given these reasonable chronostratigraphic constraints, as well as the dominance of marine organic matter, this organic-rich interval can be correlated to the Tethyan organic-rich interval (Selli Level) and considered in a strict sense as the sedimentary expression of OAE1a[13,17] (Fig. 2). The high-resolution carbon isotope stratigraphy record[11–13] (Supplementary Table S1) confirmed that the peak of organic carbon burial in Core 70 partially overlaps but mainly post-dates a negative carbon isotopic excursion (CIE) ($\delta^{13}C$ segment Ap3–Ap4). By assuming a constant sedimentation rate throughout OAE1a, the duration of the negative CIE can be estimated to be ~300–400 kyr, which roughly corresponds to the previous estimate based on cyclostratigraphy (~370 kyr[18]). As noted above, several tuffaceous limestone intervals are present in the lower Aptian sequence at Site 463 (~628.2–587.3 mbsf), and a major such interval crosses the Core 71/70 boundary (~623.46 to 621.4 mbsf)[16] (Figs. 2, 3).

Previous studies reported detailed secular Os isotope variations across OAE1a and OAE1b at DSDP Site 463[11,19]. We use these data in combination with newly generated data to complete the high-resolution Aptian Os isotope stratigraphy in the central Pacific (Fig. 2 and Supplementary Table S2). The pre-OAE1a interval at this site is characterized by a large shift in seawater $^{187}Os/^{188}Os$ from the background level of ~0.5 to the highly non-radiogenic ratio of ~0.2 (Bottini et al.[11] and this study). Extremely low $^{187}Os/^{188}Os$ ratios (~0.15) are recorded in the negative CIE. Above the OAE1a interval, $^{187}Os/^{188}Os$ ratios gradually shift to more radiogenic values (~0.5), and this shift continues to the Aptian–Albian boundary. The Aptian Os isotopic trend at DSDP Site 463 is mostly consistent with trends reported in Tethyan regions[4,11,20]. The lack of small-scale Os isotopic shifts toward the lower ratios associated with regional oceanic anoxic events reported in the Tethys (i.e., the Wezel and Fallot Events), may maybe due to non-recovery in coring gaps (Fig. 2).

Provenances of volcanic ash at DSDP Site 463

The Pb isotope data from the silicate fractions of tuffaceous layers at Site 463 (Fig. 2) are highly intriguing because all three studied Pb isotopic systems ($^{206}Pb/^{204}Pb_i$, $^{207}Pb/^{204}Pb_i$, and $^{208}Pb/^{204}Pb_i$: Supplementary Table S3 and Supplementary Fig. S1) shift towards less radiogenic values in concert with the negative CIE and Os isotope shift. However, in an expanded view (Fig. 3), a meaningful offset of the Pb isotope anomaly is discernible relative to the $\delta^{13}C_{carb}$ and Os isotope shifts. To facilitate discussion, we define two phases within the CIE: (1) CIE(OIS) is the phase when the Os isotope ratio is shifting toward lower values (~625.0–623.3 mbsf), and (2) CIE(OIB) is the phase characterized by low bottom Os isotope ratios (623.3–621.25 mbsf) (Fig. 3).

The Pb isotope compositions in the pre-CIE (gray triangles), CIE(OIS) (blue diamonds), and post-CIE (black circles) phases plot within or close to the data field for continental dust[21,22] (Fig. 4). By contrast, the data associated with the CIE(OIB) phase that spans the major tuffaceous limestone interval (~623.46–621.4 mbsf) are distinctly shifted toward less radiogenic Pb isotopic compositions (yellow and red squares in Figs. 2–4 and Supplementary Fig. S2). This variation is well illustrated by the $^{207}Pb/^{206}Pb_i$–$^{208}Pb/^{206}Pb_i$ plot (Fig. 4c), which shows the data trending obliquely to the continental dust trend and instead sub parallelling the OJP–HP–MP data array.

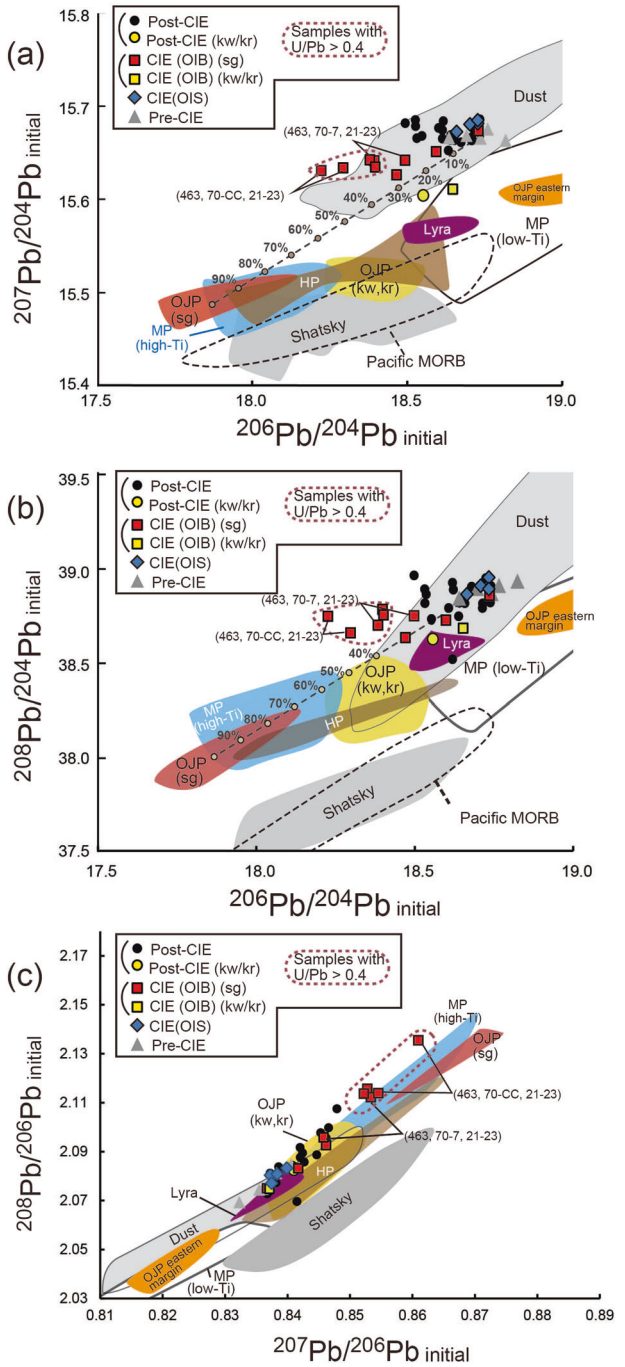

Fig. 4 | Cross plots of Pb isotopic data. a $^{206}Pb/^{204}Pb_i$–$^{207}Pb/^{204}Pb_i$, **b** $^{206}Pb/^{204}Pb_i$–$^{208}Pb/^{204}Pb_i$, and **c** $^{207}Pb/^{206}Pb_i$–$^{208}Pb/^{206}Pb_i$ from DSDP Site 463 (this study), superposed on data fields of continental dust[21,22], Shatsky Rise[79,80], Hikurangi Plateau (HP)[34], Kroenke (kr) type basalt of Ontong Java Plateau (OJP)[81], Kwaimbaita (kw) type basalt of OJP[81], Singgalo (sg) type basalt of OJP[33,81], OJP eastern margin[82], Lyra[83], and Manihiki Plateau (MP)[29,34,35,84,85]. Because it is difficult to determine the Pb isotopic values of Cretaceous continental dust, we showed those modern Asian dust and potential South American dust source[21,22] for reference. Pb isotopic ratios of Pacific Mid-Ocean Ridge Basalt (MORB) are based on ref. 86. The Pb isotopic data of dust have been corrected to 120 Ma by using U/Pb = 0.1315 and Th/Pb = 0.5861[87]. The dashed lines in **a** and **b** represent mixing lines between average Pb isotopic compositions of sg-type OJP basalt and those of silicate fractions of pre-CIE sedimentary rocks from DSDP Site 463. See Figs. 2 and 3 for the data classification with respect to CIE.

Post-depositional processes may explain the shift to less radiogenic Pb isotope signals during the CIE. Some published non-leached Pb isotopic compositions of altered kw-OJP volcanic glasses from the Eastern Salient and Nauru Basin exhibit extremely non-radiogenic values (Supplementary Fig. S3)[23–25], which have been attributed to a secondary alteration. Cenozoic to Late Cretaceous seawater generally has more radiogenic Pb isotopic compositions than these basaltic rocks[26]. Thus, interaction with hydrothermal fluids with unradiogenic Pb isotopic value may have caused such a shift to lower, unradiogenic Pb compositions. However, unlike in the previous studies, the hydrogenous fraction was removed by CH_3COOH and HCl leaching before the Pb isotopic analysis. In addition, the measured and initial Pb isotopic compositions of our samples show similar stratigraphic variations with small age corrections throughout the section (Supplementary Fig. S1). We therefore deduce that the observed Pb isotopic variations mostly reflect the original Pb isotopic signals of the silicate fractions. However, we also note that the reproducibility of U/Pb within the tuffaceous interval, CIE(OIB), (463_70-7_21-23 and 463_70-CC_21-23) is not good (Supplementary Table S3), and there is a negative correlation between $^{206}Pb/^{204}Pb_i$ and U/Pb ratios ($r^2 = 0.75$) (Supplementary Fig. S4). The anomalously low values and negative correlation are especially obvious for samples with high U/Pb ratios (>0.4) (Fig. 4). Because U/Pb is used for the age corrections of $^{206}Pb/^{204}Pbi$, variations of U/Pb ratios due to insufficient leaching of hydrogenous *U* could have caused the over age corrections of $^{206}Pb/^{204}Pb$, particularly in samples with U/Pb ratios >0.4. Nevertheless, even when excluding these samples with high U/Pb ratios, the shift to the unradiogenic $^{206}Pb/^{204}Pb$ values remains obvious for the remaining data (Fig. 4). In contrast to the negative correlation of $^{206}Pb/^{204}Pb_i$ with U/Pb ratios, no meaningful correlations were observed in $^{207}Pb/^{204}Pb_i$–U/Pb and $^{208}Pb/^{204}Pb_i$–Th/Pb for samples with U/Pb ratios <0.4 (Supplementary Fig. S4). The lack of correlation indicates that the impact of age-correction is minor compared to the inherent variations in $^{207}Pb/^{204}Pb_i$ and $^{208}Pb/^{204}Pb_i$ values between samples[27].

The subparallel trend of the silicate fraction data to the OJP data array in the $^{207}Pb/^{206}Pb_i$–$^{208}Pb/^{206}Pb_i$ plot, and the systematic variation in the $^{206}Pb/^{204}Pb_i$–$^{207}Pb/^{204}Pb_i$, and $^{206}Pb/^{204}Pb_i$–$^{208}Pb/^{204}Pb_i$ cross plots, may indicate variable inputs from the OJN volcanism. First, the Pb isotope composition of the lowest sample from the major tuffaceous limestone (i.e., the oldest sample in the CIE(OIB) phase: 623.37 mbsf: yellow square in Figs. 2–4) is noteworthy for plotting close to the fields of the kw/kr-type OJP, HP, Nauru Basin, Shatsky Rise, low-Ti MP, and Pacific oceanic ridge basalts. Of these, the kw/kr-type OJP basalt is the dominant rock type of the OJN. Subaerially erupted volcanic clasts that are compositionally similar to kw-type basalt are known from the Eastern Salient of OJP[24,28] and hyaloclastites with kw-type chemical composition are present in the sedimentary sequences in the Nauru Basin (DSDP Site 462) and East Mariana Basin (Ocean Drilling Program [ODP] Site 802)[23] (Fig. 1). Furthermore, the Pb isotopic compositions of the lowest tuffaceous sample are similarly close to those of low-Ti basalts, one of the major basalt types on MP[29] (Fig. 4). OJP source-derived younger Lyra Basin basalts also exhibit similar Pb isotopic composition to the lowest tuffaceous sample (Fig. 4). These observations suggest that the most probable sources of the lowest ash layer in the main tuffaceous interval (623.37 mbsf) were kw/kr-type OJP and/or low-Ti type MP magma although limited evidence suggests that subaerial eruption may have occurred during the main phase of OJP formation.

In contrast, the Pb isotope compositions of samples from the main part of the major tuffaceous limestone interval (in the CIE(OIB) phase) plot toward those of the sg-type OJP basalt or the high-Ti type MP basalt (623.01–621.40 mbsf: red squares in Figs. 2–4 and Supplementary Fig. S2). Some samples show anomalously unradiogenic isotopic ratios compared to the sg-type OJP basalt. As explained above, these unradiogenic values could be artifacts of over-age corrections due to modified U/Pb ratio of the original silicate fraction. Nevertheless, even when excluding samples with high

U/Pb ratios (>0.4), the trend towards the sg-type basalt can be observed (e.g., 463_70-6_50-52) (Supplementary Table S3), which still supports our suggestion that the Pb isotopic composition of volcanic ash approach that of sg-type OJP basalt. The geochemical features of the sg-type OJP basalt and the high-Ti-type MP basalt are almost identical, and they may have been derived from a similar magma source[29]. Notably, some high-Ti basalts on the MP (High Plateau: DSDP Site 317) may have formed at shallow water depths or even subaerially[30]. Therefore, we conclude that volcanic eruptions of sg-type OJP or high-Ti-type MP magmas were likely responsible for the marked Pb isotope anomaly within the CIE(OIB) phase. Indeed, a vitric tuff with a sg-type chemical composition has been reported from Site 1183 on the High Plateau of OJP (Fig. 1 and Supplementary Fig. S3). In addition, the Pb isotopic compositions of the silicate fraction from coeval sedimentary rocks on Shatsky Rise (ODP Site 1207) also show a shift toward an sg-type OJP basalt/high-Ti MP basalt composition, suggesting input of OJN-sourced volcanic ash (Fig. 1 and Supplementary Fig. S3)[10]. These sedimentary rocks may correlate with the sg-like volcanic ash layer at DSDP Site 463. A mixing model was constructed to estimate the potential effect of sg-type ash fallout contribution to Pb isotopic composition of silicate fractions in the normal pelagic sedimentary rocks, assumed to be compositionally similar to pre-CIE samples (Figs. 3 and 4). The results show that the isotopic composition of the silicate fractions in CIE(OIB) sedimentary rocks from DSDP Site 463 can be explained by ~30% input of sg-type OJN basaltic materials.

To summarize the foregoing, the occurrences of the volcanic ash layers and the unique Pb isotopic data at Site 463 strongly suggest the presence of volcanic material derived from explosive subaerial or shallow-marine eruptions at OJN during the CIE(OIB) phase. Interestingly, the Pb isotopic signal of kw/kr-type basalts, which are the dominant type on OJP, is limited to the lowest part of the major tuffaceous limestone (yellow square in Figs. 2–4), whereas the main part of the major tuffaceous limestone exhibits Pb isotope signals of the later-erupted sg-type OJP or high-Ti MP basalts (red squares in Figs. 2–4).

One probable explanation for this Pb isotopic trend is changes in the eruption style of OJN. According to present knowledge, the kw/kr-type basalt was emplaced during the early stage of OJP volcanism, when most of the volcanic edifice was forming under submarine conditions[31], possibly 500 to 3000 m below the sea surface (Fig. 5). An eruption in such a deep-sea setting is unlikely to release volcanic ash over a vast area. However, shallow to subaerial phreatomagmatic eruptions on the OJP at this time cannot be ruled out, as exemplified by petrified wood and volcaniclastic deposit occurrences on its Eastern Salient[28]. Such explosive style of eruption is also capable of widespread dispersion of volcanic ash. For example, in the case of the North Atlantic Magmatic Provinces (NAIP), a large amount of volcanic ash was released by phreatomagmatic eruptions and was documented ~1900 km away from the volcanic center[32]. Hence, phreatomagmatic eruption of kw/kr-type magma on the OJP's Eastern Salient[24,25,28] or elsewhere on the High Plateau might have been the source of the lower part of the major tuffaceous limestone interval in DSDP Site 463 (Figs. 2 and 3).

During the later volcanic stages, sg-type OJP/high-Ti MP basalt erupted atop the kw/kr-type OJP/low-Ti MP basalts (Fig. 5)[29,33]. This later volcanism certainly occurred at shallower depths, or even under subaerial conditions when the main edifices of both OJP and MP have already been emplaced, and may have released a large amount of volcanic ash into the atmosphere (Fig. 5). Indeed, the High Plateau of the MP consisting of high-Ti type basalt is suggested to have been formed under subaerial condition[30]. It should be noted that the timing of this explosive sg-like magma eruption is

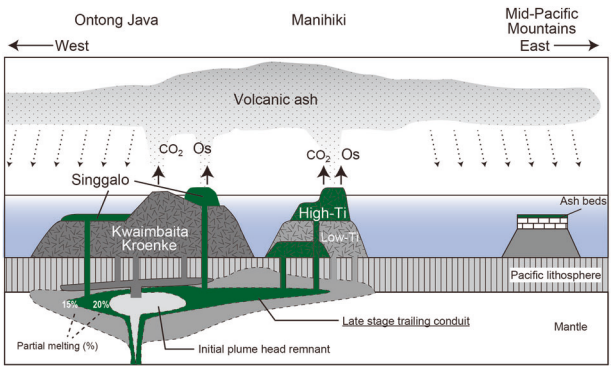

Fig. 5 | Schematics diagram of Ontong Java Nui volcanism at the explosive subaerial/shallow-marine eruption phase corresponding to CIE(OIB). The volcanic ash and Os-bearing volatiles originate from a volcanic eruption that formed sg-type OJP and high-Ti-type MP basalts.

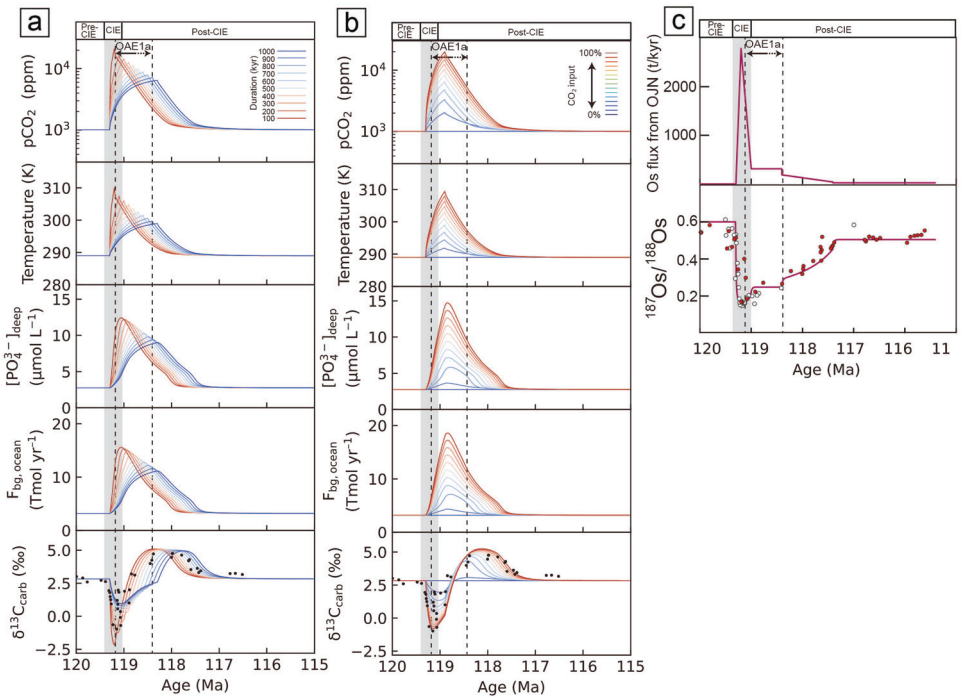

Fig. 6 | Results of the model calculations. This figure shows burial rate of organic matter in the ocean [$F_{bg,ocean}$], phosphorus, temperature, and pCO_2 to the injection of CO_2 estimated using the C–P biogeochemical model (**a**, **b**) and mantle-derived Os input estimated using the Os box model (**c**). **a** The duration of the input of CO_2 is varied from 100 to 1000 kyr, and in **b**, the amount of CO_2 input is varied from 0 to 10^{22} g CO_2 (~2.7×10^5 GtC), during 400 kyr, which is the estimated maximum amount of CO_2 released from OJP[42]. Data points in **a** and **c** represent the actual data from DSDP Site 463.

uncertain, because high-Ti basalts with sg-type compositions occurred on MP both from its shallowest part[34] to the deeper section[29,35]. This potentially deeper sg-like magma eruption on MP may imply a somewhat earlier onset of the OJN volcanism that formed the high-Ti-type MP basalts.

An alternative source of volcanic ash at DSDP Site 463 could be the small volcanic chains that were also active around 120 Ma[36]. However, these small-volume hot-spot volcanic activities continued for several tens of million years[36], while the volcanic ash layer of DSDP Site 463 is limited to a specific interval around the OAE1a. Moreover, previously reported Pb isotopic composition for these Cretaceous ocean island basalts is highly radiogenic (e.g., $^{206}Pb/^{204}Pb > \sim 20$)[27,37], inconsistent with the trend of the Pb isotopic data for the tuffaceous interval (Fig. 4). Therefore, we consider such small hot-spot volcanic activities as unlikely source of volcanic ash at DSDP Site 463. Explosive volcanic eruption of felsic magma from the volcanoes in nearby subduction zone could be another candidate for the source of volcanic ash in the Pacific regions. However, no such active arc volcanic activity during the Barremian–Aptian was reported so far. For example, among the well-studied Japanese granites, Aptian felsic rocks are very limited[38] and such arc volcanism was more active at a later time[39]. Also, similar early Aptian volcanic events associated with the subduction of Pacific Plate have been reported from China, but the compilation of the U-Pb ages suggests that the peak of volcanic events occurred at ~100, 113, and 128 Ma, which are different from the timing of volcanic ash occurrences[40]. Therefore, we consider that these volcanic events were not the source of large emissions of CO_2 and volcanic ash. Due to the lack of other possible candidates, we conclude that volcanic eruption on the OJN is the most probable source of the volcanic ash layers.

A possible complication is that the latest $^{40}Ar–^{39}Ar$ ages reported for OJP basalts, previously dated to older than ~120 Ma, range from the late Aptian to Albian (~117–108 Ma)[9]. However, studies of planktonic foraminifera and calcareous nannofossil assemblages in limestone samples from the plateau suggest that the majority of OJP (including the same cores from which the dated basalts were sampled) was formed by early to mid-Aptian[7,8], and these ages are consistent with the sedimentary ages of volcanic ash in Pacific regions. Although the discrepancy between the radiometric and biostratigraphic ages presents a conundrum, it is reasonable to consider that the volcanic ash layers were derived from OJP and MP, which collectively comprise OJN volcanism.

Modeling C, P, and Os cycles in response to OJN volcanic events

The close coincidence between the peak submarine-to-subaerial OJN volcanism (as corroborated by the Pb and Os isotopes) and the CIE suggests that a release of isotopically light carbon, caused by degassing of volcanic CO_2 with very negative $\delta^{13}C$ values (~−6‰[41]), occurred only during the shallow-marine/subaerial volcanic phase at OJN (Fig. 2). We employed a simplified biogeochemical box model (Supplementary Fig. 6) to simulate the response of the global C and P cycles to the volcanism caused by OJN eruptions. The test, which considered various levels of total C influx and durations of the volcanism (Fig. 6), demonstrated that the negative and subsequent positive $\delta^{13}C$ variations across OAE1a can be reasonably explained by injecting $\sim 1.93 \times 10^5$ GtC during the first ~400 kyr of the volcanism (Fig. 6a, b). This estimate does not take account of other sources with extremely negative $\delta^{13}C$ values (such as methane hydrate or sediment-hosted methane); therefore, it reflects an extreme scenario of volcanic degassing only. Currently, there are no available CO_2 data from the original OJN melt inclusion, probably due to degassing during the ascent of magma[31]. Nevertheless, assuming the estimated volume of OJN as $\sim 5 \times 10^7$ km^3 (including the extrusive and intrusive parts) and the CO_2 concentration of the original melt of tholeiitic basalts as 7000 ppm, the maximum estimation of released carbon is $\sim 2.75 \times 10^5$ GtC[42]. Therefore, our estimation falls within an acceptable range of that estimated from the OJP volume[42]. This short but intensive CO_2 emission scenario is also supported by other modeling studies[43].

The Os isotopic record indicates that a large amount of non-radiogenic Os was released from OJN during the CIE. In theory, the seawater $^{187}Os/^{188}Os$ ratio represents the balance of inputs between mantle/extra-terrestrial non-radiogenic Os ($^{187}Os/^{188}Os = \sim 0.12$) and continental radiogenic Os ($^{187}Os/^{188}Os = 1.0–1.5$) into the ocean reservoir. On the basis of the broad agreement between the radiometric ages of OJN and the standard chronology of OAE1a, the non-radiogenic Os isotope shift during the early Aptian has been linked to an input of mantle-derived Os through the OJN volcanism[4,11]. The $^{187}Os/^{188}Os$ ratios fell to non-radiogenic values (~0.15) during the negative CIE (Figs. 2 and 3), suggesting that the largest contribution of mantle-derived Os occurred at that time (Fig. 6c). Our Os box model calculation indicated that $\sim 6.4 \times 10^9$ t Os was released from OJN during the Os isotopic bottoming-out around OAE1a, with 70% of that being emitted during the negative CIE (Fig. 6c). The important question now is how such a large amount of Os was emitted into the ocean reservoir.

One possible source of the Os release is subaerial weathering of the basaltic plateaus, but most of OJN was emplaced under submarine conditions[31]. The only known evidence for a subaerial eruption is on OJP's Eastern Salient[28] and on the Manihiki High Plateau[30]. To explain the non-radiogenic shift solely by weathering of the Eastern Salient and MP basalt flows, an unrealistically large volume of basaltic rock body (an area of $\sim 1 \times 10^6$ km^2 and a height of 10–20 km) would need to have been weathered away within ~1 million years.

Another possibility is that hydrothermal activity during the interaction of seawater and basaltic lava[4,11]. However, Sharma et al.[44] indicated that the Os concentration of present-day hydrothermal fluids is too low to explain the total amount of mantle-derived non-radiogenic Os emissions. In addition, assuming that OJN had a total area of $\sim 5 \times 10^6$ km^2[2,1], an average height of ~3.6 km[29], and an average Os concentration of ~100 ppt, almost all Os in the erupted part of OJN would need to have been leached out hydrothermally. Notably, the Re-Os system of OJP basalt is reported to have remained largely a closed system[45]. Thus, the hydrothermal emission of mantle-derived Os is unlikely by itself to explain the non-radiogenic shift of $^{187}Os/^{188}Os$.

The last and most plausible possibility is Os emission as volatiles associated with volcanic eruption and degassing[46]. Os is a highly volatile element when oxidized. Given that the timing of Os emission corresponded to a volcanic CO_2 input during the negative CIE (Figs. 2, 3, and 6), a large amount of volatile Os could have been released during the explosive volcanic phase along with other volatiles. Indeed, some mantle xenoliths from the deeper part of the OJP (>95 km) were found to have extremely low Os concentrations[47]; this result implies that a large amount of Os was fractionated into the melt as an incompatible element. In addition, primary OJP magmas might have formed under relatively oxidized conditions because of recycling of oceanic crust[48]. Under such redox conditions, the mantle might have effectively hosted oxidized Os that was eventually transported into the ocean–atmosphere system with other volatiles. Although further research on the exact oxidation process of Os is essential, we consider volcanic degassing as the most important process for the release of a large amount of mantle-derived volatile Os during the CIE.

As noted in the previous section, the Pb isotopic composition of silicate fractions from the tuffaceous limestones is influenced by sg-type OJP/high-Ti type MP. The sg-type basalts appear to be volumetrically minor on OJP, and it is unclear if the volcanic eruptions forming these basalts (Fig. 5) could release a large amount of volatiles. Meanwhile, outpouring of high-Ti (sg-like) basalts on MP appears to have occurred throughout the plateau's formation[29] and may have culminated in subaerial eruptions, as has been reported from DSDP Site 317 on the High Plateau[35]. Speculatively such sg-like explosive eruptions may have also taken place during the initial stages of OJP formation. Direct evidence for the occurrence of a volatile-enriched volcanic eruption at the OJP is currently lacking, but our results, combined with volcanic stratigraphy on MP[29,30], indicate that such event may have taken place during the initial emplacement of the plateau complex prior to OAE1a event.

Possible cause of the time lag between the explosive OJN volcanism and OAE1a

The linkage between LIP volcanism and the onset of OAEs has been long debated. The proposed triggering mechanism is as follows: volcanic

degassing caused global warming and enhanced continental weathering, which led to ocean eutrophication and eventually caused an increase in primary productivity[7]. The Site 463 C, Os, and Pb isotopic data demonstrate that a volcanic degassing event associated with explosive subaerial/shallow-marine OJN volcanism occurred during the CIE(OIB) (Fig. 3), and this event may have triggered an increase in primary productivity. Indeed, our biogeochemical model projected that the accumulation of atmospheric CO_2 caused by the eruption of OJN resulted in a sharp increase in surface temperature (>5 K) and, hence, eutrophication of the ocean. Our best estimate predicts a nearly two-fold increase in marine P concentrations. However, intriguingly, the TOC contents of the tuffaceous limestone interval are low (~0.27% on average), and they sharply increase after the end of the major tuffaceous limestone interval (Fig. 3). One possible explanation for the time lag between the tuffaceous interval (i.e., explosive volcanic eruption) and the organic-rich interval (i.e., OAE1a) might be differences in the sedimentation rate during the two intervals. If the tuffaceous limestone interval was deposited at an unusually high sedimentation rate, the TOC contents would have been lowered as a result of dilution of organic carbon in the sediments; however, this possibility cannot explain the similarly low TOC contents in the non-tuffaceous intervals deposited during the degassing event (~625–623.5 and ~623.1 mbsf) (Fig. 3).

Alternatively, this time lag may reflect the oceanic response time between the peak of the degassing event at OJN and the development of eutrophic conditions sufficient to increase the primary productivity in a Pacific open-ocean setting. Indeed, our C–P biogeochemical model calculation indicated that the peak of ocean eutrophication (i.e., the peak phosphorus concentration in seawater) occurred after the degassing event (Fig. 6). Therefore, we propose that a threshold amount of ocean eutrophication must be reached before an abrupt increase in primary productivity occurs, and that oceanic conditions in the Pacific only reached this threshold during the late stage of explosive subaerial/shallow-marine volcanic eruptions. In some Tethyan sedimentary sequences (e.g., the Cau core, Spain[49]; and the Cismon core, Italy[50]), TOC increased sharply immediately after the onset of the CIE (i.e., the onset of the degassing event). However, because these Tethyan sedimentary sites are closer to the continent than Site 463, these sections might have achieved the threshold more quickly than pelagic Pacific sites.

Even after the intensive degassing event, the interval with high TOC content continued for several hundred kiloyears, until the end of OAE1a. This prolonged period of organic carbon burial after the main degassing event suggests that more than several hundred kiloyears are required to restore nutrient conditions in the ocean to the background level. Indeed, our C–P biogeochemical model calculations confirmed that high P concentrations and enhanced organic carbon burial continued even after OAE1a (Fig. 6). An alternative explanation is that minor volcanic events continuing after the main volcanic pulse continuously released CO_2 and caused the prolongation of OAE1a. At DSDP Site 463, intermittent volcanic ash layers have been reported until the lower part of the upper Aptian (Core 67)[16] (Fig. 2). In addition, Os isotopic ratios were persistently as low as ~0.2 until the end of, or even after, OAE1a[20]. These pieces of evidence suggest that minor volcanic events at OJN continuing after the main degassing event may have contributed to the continuously high amount of organic carbon burial. Although further understanding of the triggering mechanism of OAEs is essential, the intensive degassing event and the delayed and prolonged OAE1a in the pelagic Pacific region provide clues to understanding the spatiotemporal response of primary productivity to massive volcanic episodes.

Method

Stable carbon isotope ratio of carbonate

The stable carbon isotope ratio of carbonate ($\delta^{13}C_{carb}$) was determined by isotope ratio-mass spectrometry (Delta V plus, Thermo Fisher Scientific, USA), equipped with an automated carbonate reaction device (GasBench II, Thermo Fisher Scientific, USA), at the Atmosphere and Ocean Research Institute, University of Tokyo (Japan). All isotope values are expressed in the delta notation with respect to PeeDee Belemnite (PDB), with an NBS-19 value of −2.20‰ for $\delta^{18}O$ and +1.95‰ for $\delta^{13}C$. The reproducibility was estimated from the repeated measurement of the NBS-19 standard within an analysis batch, which is typically better than 0.07‰ and 0.09% for $\delta^{18}O$ and $\delta^{13}C$, respectively (1 SD) (Supplementary Table S1).

Re- and Os analysis

Cleaned samples were dried and powdered in an agate mill. After spiking with ^{190}Os and ^{185}Re-rich solutions, powdered samples were sealed in the Carius tube[51] with 4 ml of inverse aqua regia (mixture of 1 ml of 30 wt% HCl and 3 ml of 68 wt% HNO_3: TAMAPURE-AA-10 from Tama Chemicals Co. Ltd., Japan). They were heated at 240 °C for 48 hours. The supernatant was separated from the residue by centrifugation. Os was separated and purified from the leachate through carbon tetrachloride extraction[52,53], HBr extraction, and microdistillation[54]. Re was separated from the leachate using Bio-Rad AG1-X8 anion exchange resin. Abundances and isotopic ratios of Os were determined by negative thermal ionization-mass spectrometry (TRITON, Thermo Fisher Scientific, Waltham, USA) equipped by Japan Agency for Marine-Earth Science and Technology (JAMSTEC, Japan). The Re abundances were determined by a quadrupole inductively coupled plasma-mass spectrometer (iCAP Qc, Thermo Fisher Scientific, USA) at JAMSTEC. The average procedural blanks of Os were 0.6 ± 0.3 pg, with $^{187}Os/^{188}Os$ was 0.12 ± 0.03. The average Re-procedural blank was 5 ± 1 pg. Initial $^{187}Os/^{188}Os$ values ($^{187}Os/^{188}Os_i$) were calculated from the measured $^{187}Os/^{188}Os$ and $^{187}Re/^{188}Os$ values, the age-depth model of the sediments (Supplementary Tables S2 and S4), and the ^{187}Re decay constant (1.666×10^{-11} yr^{-1})[55]. Detailed analytical methods for Os isotopic analysis were as described by ref. [19].

Lead isotopic analysis

The powdered sedimentary rock samples (ca. 1 g) were reacted with acetic acid (30%, TAMAPURE-AA-10 from Tama Chemicals Co. Ltd., Japan) in Savillex® PFA vial and they were immersed in an ultrasonic bath for 30 minutes to remove carbonate. We repeated the process several times. After the supernatant was removed by centrifugation, the residues were soaked in 1 M HCl and heated at 80°C for a few hours. For carbonate-rich samples, the residues were soaked in 5 ml of 6 M HCl for several minutes to remove carbonate completely. After removing HCl by centrifugation, the residues were rinsed several times with ultrapure water, which was purified and deionized with Milli-Q® water system (Merck Millipore). The residues were then decomposed with 3.0 ml of HF (38%, TAMAPURE-AA-10 from Tama Chemicals Co. Ltd., Japan) and 1 mL of HNO_3 (68%, TAMAPURE-AA-10 from Tama Chemicals Co. Ltd., Japan), heated in an electric oven at 110 ˚C for 24 hours, followed by heating at 120 ˚C for 24 hours for complete decomposition. The decomposed samples were evaporated to dryness, and the residues were dissolved in 4 ml of 30% HCl. A portion of this solution was diluted with 3% HNO_3 to determine their U, Pb, and Th concentrations. The concentrations were determined with the quadrupole inductively coupled plasma mas-spectrometry (ICP-MS) (Agilent 7500cx; Agilent Technologies Japan Ltd., Japan) equipped in the Geological Survey of Japan (GSJ). Drift and matrix corrections were applied using the ^{209}Bi internal standard intensities. After the quantitative determination of U, Pb, and Th, the remaining solution was evaporated to dryness and redissolved with 0.5 M HBr. The sample solutions were passed through 400 µl of 100–200 mesh anion exchange resin (AG MP-1M, Bio-Rad Laboratories, USA) packed in polypropylene columns (Bio-Spin® column, Bio-Rad Laboratories, USA) to separate Pb based on the method described in ref. 56 All experimental procedures were conducted in a clean room at the GSJ. The Pb isotope ratios were determined using the multi-collector ICP-MS (NEPTUNE, Thermo Fisher Scientific Inc., USA) equipped in GSJ. Pb isotopic ratios were determined using a Tl spike, NIST SRM 997, and sample–standard bracketing. The Pb isotopic compositions of the bracketing NIST SRM981 standards were assumed to be 16.9412 for $^{206}Pb/^{204}Pb$, 15.4988 for $^{207}Pb/^{204}Pb$, 36.7233 for $^{208}Pb/^{204}Pb$ ratio[57]. The

reproducibility of Pb isotopic analysis was confirmed by the repeated analysis of JB2-1 (not leached). Pb isotopic values of JB2-1 were $^{206}Pb/^{204}Pb = 18.3415 \pm 0.0023$, $^{207}Pb/^{204}Pb = 15.5612 \pm 0.0085$, $^{208}Pb/^{204}Pb = 38.2744 \pm 0.0224$ ($n = 3$, 2 SD), which is good agreement with the previously reported values ($^{206}Pb/^{204}Pb = 18.3435 \pm 0.0017$, $^{207}Pb/^{204}Pb = 15.5619 \pm 0.0016$, $^{208}Pb/^{204}Pb = 38.2784 \pm 0.0050$)[58]. Average U, Th, Pb concentrations of JB2 are 0.16, 0.28, 4.97 ppm ($n = 2$), which is consistent with the previously reported values (0.1528 ± 0.0028, 0.2576 ± 0.0048, and 5.25 ± 0.11)[59]. During the analytical session, we also determined the isotopic compositions of SRM981 by standard bracketing combined with Tl doping. Their average values were $^{206}Pb/^{204}Pb = 16.9413 \pm 0.0019$, $^{207}Pb/^{204}Pb = 15.4990 \pm 0.0020$, and $^{208}Pb/^{204}Pb = 36.7236 \pm 0.0055$ ($n = 5$, 2 SD). The Pb isotopic ratios were corrected by the age (120 Ma) using U/Pb for $^{206}Pb/^{204}Pb_i$ and $^{207}Pb/^{204}Pb_i$ and Th/Pb for $^{208}Pb/^{204}Pb_i$.

Global C–P biogeochemical modeling

Biogeochemical Model. We developed a biogeochemical model that estimates a short-term fluctuation of the system following the ocean–atmosphere eruption of the Ontong Java Nui. The model estimates the time evolution of the amount of atmospheric CO_2, oceanic dissolved inorganic carbon (DIC), oceanic phosphorus (P), oceanic calcium (Ca), soil and vegetation carbon on land, and ^{13}C when the system is forced with a CO_2 influx assuming the eruption of the Ontong Java Nui. In this model, the ocean is represented by one box for the DIC and Ca cycles and three boxes for the P cycle (Supplementary Fig. S6). The budgets of atmospheric CO_2, *DIC*, and Ca^{2+} in the ocean are represented as follows:

$$\mu_{atm}\frac{d}{dt}(pCO_2) = F_{ao} + F_{wg} + F_{mc} + F_{mg} - F_{ws} - F_{wc} - F_{nep,land} \quad (1)$$

$$V_{oc}\frac{d}{dt}([DIC]) = F_{OJN} - F_{ao} + F_{ws} + 2F_{wc} - F_{bg,ocean} - F_{pc} \quad (2)$$

$$V_{oc}\frac{d}{dt}\left(\left[Ca^{2+}\right]\right) = F_{wc} + F_{ws} - F_{pc}, \quad (3)$$

where F_{ao} is the gas exchange rate of CO_2 from ocean to atmosphere; F_{mc} and F_{mg} are the degassing rate from volcanism, metamorphism, and diagenesis of carbonates and organic carbon, respectively; F_{wg} is the production rate of CO_2 from the weathering of land organic carbon; F_{ws} is the silicate weathering rate; F_{wc} is the carbonate weathering rate; $F_{nep,land}$ is the net ecosystem productivity on land; F_{OJN} is the volcanic outgassing rate of CO_2 owing to the eruption of the Ontong Java Nui; $F_{bg,ocean}$ is the burial rate of organic carbon from the ocean; F_{pc} is the deposition rate of calcium carbonate from the ocean; V_{oc} is the mass of the ocean ($V_{oc} = 1.4 \times 10^{21}$ L); and μ_{atm} is the number of moles in the present atmosphere ($\mu_{atm} = 1.773 \times 10^{20}$ mol). The choices of the parameters are summarized in Supplementary Method and Supplementary Table S5.

The global-mean surface temperature is estimated using a zero-dimensional energy balance model[60], which considers the balance between the incoming solar radiation and the outgoing longwave radiation to space considering the greenhouse effect from CO_2 and H_2O:

$$(1 - \alpha(T_s)) \cdot \frac{S(t)}{4} = F_{OLR}(T_s), \quad (4)$$

where α is the top-of-atmosphere albedo of the Earth, and F_{OLR} is the outgoing longwave radiation flux, both of which are a function of T_s[61], and S(t) is the solar constant at *t* million years ago (W m^{-2}), which is formulated as follows[62]:

$$S(t) = S_0 \cdot \left(1 - 0.38\frac{t\,(Ma)}{4550}\right)^{-1} \quad (5)$$

The budget of phosphorus (PO_4^{3-}) in the ocean is represented by three oceanic boxes, as follows:

$$V_l\frac{d}{dt}([PO_4^{3-}]_l) = f_l F_{rp} + F_{adv,ds} - F_{adv,sh} + F_{dif,ds} - F_{dif,sh} - \frac{1}{R_{cp,bio}}F_{po,l} \quad (6)$$

$$V_h\frac{d}{dt}([PO_4^{3-}]_h) = f_h F_{rp} + F_{adv,sh} - F_{adv,hd} + F_{dif,sh} - F_{dif,hd} - \frac{1}{R_{cp,bio}}F_{po,h} \quad (7)$$

$$V_d\frac{d}{dt}([PO_4^{3-}]_d) = \frac{1}{R_{cp,bio}}F_{po} - \frac{1}{R_{cp,sed}}F_{bg} - F_{FeP} - F_{CaP} + F_{adv,hd} - F_{adv,ds} + F_{dif,hd} - F_{dif,ds}, \quad (8)$$

where F_{rp} is the riverine phosphorus supply rate; $F_{adv,ij}$ and $F_{dif,ij}$ are the oceanic exchange rate of P from box *i* to box *j* via thermohaline circulation and diffusion, respectively; f_l and f_h are the areal fraction of the low-latitude and high-latitude surface water boxes, respectively ($f_l = 0.85$ and $f_h = 0.15$); V_l and V_h are the mass of surface ocean boxes at low and high latitudes, respectively ($V_l = 3.06 \times 10^{19}$ L and $V_h = 0.54 \times 10^{19}$ L); V_d is the mass of deep ocean ($V_d = 1.364 \times 10^{21}$ L); F_{FeP} and F_{CaP} are the burial flux of Fe-bound P, and Ca-bound P, respectively; R_{cp} is the C:P ratio of marine biomass ($R_{cp,bio} = 106$); and $R_{cp,sed}$ is the C:P ratio of organic carbon buried in sediments, which is represented as a function of the anoxic fraction of the ocean (f_{anox})[63]:

$$R_{cp,sed} = \frac{R_{cp,ox}\,R_{cp,anox}}{(1 - f_{anox})R_{cp,anox} + f_{anox}\,R_{cp,ox}}, \quad (9)$$

$$f_{anox} = \frac{1}{1 + \exp\left(-12\left(\frac{0.5(F_{po,s}+F_{po,h})}{F_{po,0}} - pO_2(PAL)\right)\right)} \quad (10)$$

where $R_{cp,ox}$ and $R_{cp,anox}$ are the C:P ratio of organic carbon in sediments under oxic and anoxic waters, respectively ($R_{cp,ox} = 250$ and $R_{cp,anox} = 400$) and pO_2 is the atmospheric oxygen level (present atmospheric level; PAL). $R_{cp,sed}$ is ~250 at the present export production flux ($F_{po,0} = 0.75$ Pmol C yr^{-1})[63]. This value approaches 400 under conditions with high export production rates. We note here that this maximum value could be much higher under extreme conditions during ocean anoxic events[63–66], which may increase the amplitude of positive carbon isotope excursions. Nevertheless, our global model with an upper limit of $R_{cp,sed}$ of 400 successfully reproduces the positive excursions. The pO_2 value is fixed at the present value ($pO_2 = 1$ PAL), which would be a reasonable value for 120 Ma condition[63].

The riverine *P* supply rate is represented as follows:

$$F_{rp} = \frac{F_{ws} + F_{wc}}{F_{ws,0} + F_{wc,0}} \cdot F_{rp,wsc,0} + \frac{1}{R_{cp,land}} \cdot (F_{wg} - F_{nep,land}), \quad (11)$$

where $F_{rp,wsc,0}$ is the present riverine *P* supply rate owing to weathering of P-hosting minerals in continental silicate and carbonate ($F_{rp,wsc,0} = 0.039$ Tmol P yr^{-1}), $R_{cp,land}$ is the C:P ratio of land organic matters ($R_{cp,land} = 1000$)[63], and $F_{nep,land}$ is the net ecosystem productivity of the land ecosystem. The riverine *P* is consumed in the surface ocean by primary producers. The export production rate of OC is represented as follows[67]:

$$F_{po,i} = \epsilon_i R_{cp,bio} \cdot V_i \cdot \left[PO_4^{3-}\right]_i \cdot \frac{[PO_4^{3-}]_i}{[PO_4^{3-}]_i + \gamma_p}, (i = s, h) \quad (12)$$

where ε is the efficiency factor for phosphorus uptake (3.0 and 0.8 for low-latitude and high-latitude surface water boxes, respectively) and γ_p is a half

saturation constant for the export production ($\gamma_p = 1.0 \times 10^{-6}$ mol L^{-1}). Using the estimated export production rate, the marine net primary productivity is calculated as follows, assuming an export production efficiency (f_{po}).

$$F_{npp,ocean} = \frac{F_{po}}{f_{po}}. \quad (13)$$

The burial rate of OC to the sediment is calculated by assuming a constant burial efficiency (defined here as the ratio between burial rate and export production rate, β_{bur}), as follows:

$$F_{bg,ocean} = \beta_{bur} \cdot F_{po}. \quad (14)$$

At a steady state, the riverine *P* supply rate is equivalent to the *P* removal rate by the deposition of OC, Fe-bound *P*, and Ca-bound *P*. The value of β_{bur} is chosen so that the present condition is reproduced in the model (See Supplementary Method). $F_{adv,ij}$ and $F_{dif,ij}$ are represented as follows, respectively:

$$F_{adv,ij} = T \cdot ([PO_4^{3-}]_j - [PO_4^{3-}]_i) \quad (15)$$

$$F_{dif,ij} = W_{dif,ij} \cdot ([PO_4^{3-}]_j - [PO_4^{3-}]_i). \quad (16)$$

where T is the thermohaline circulation flux and $W_{dif,ij}$ is the diffusive exchange flux between ocean boxes i and j ((i,j) = (s, h), (h, d), (d, s)) The Fe-bound and Ca-bound *P* burial fluxes are represented as follows, respectively[63]:

$$F_{FeP} = F_{FeP,0}\left(\frac{[PO_4^{3-}]_d}{[PO_4^{3-}]_{d,0}}\right)(1 - f_{anox}). \quad (17)$$

$$F_{CaP} = F_{CaP,0}\left(\frac{F_{bg,ocean}}{F_{bg,ocean,0}}\right). \quad (18)$$

where $F_{FeP,0}$ and $F_{CaP,0}$ are the present values ($F_{FeP,0}$ = 0.01 Tmol *P* yr^{-1} and $F_{CaP,0}$ = 0.02 Tmol P yr^{-1}), respectively[63].

C isotope budgets. The budget of ^{13}C is represented as follows:

$$\begin{aligned}\frac{d}{dt}(^{13}C_{atm}) =& f_{13C,oa}F_{ao,\uparrow} - f_{13C,ao}F_{ao,\downarrow} + f_{13C,g}F_{wg} \\ &+ f_{13C,c}F_{mc} + f_{13C,g}F_{mg} - f_{13C,atm}(F_{ws} + F_{wc}) \\ &- (f_{13C,bg}F_{gpp,land} - f_{13C,veg}F_{res,land} - f_{13C,soil}F_{htr,land})\end{aligned} \quad (19)$$

$$\begin{aligned}\frac{d}{dt}(^{13}C_{ocean}) =& f_{13C,OJN}F_{OJN} + f_{13C,ao}F_{ao,\downarrow} - f_{13C,oa}F_{ao,\uparrow} + f_{13C,atm}F_{ws} \\ &+ (f_{13C,atm} + f_{13C,c})F_{wc} - f_{13C,bg}F_{bg,ocean} - f_{13C,pc}F_{pc}\end{aligned} \quad (20)$$

$$\begin{aligned}\frac{d}{dt}(^{13}C_{veg}) =& f_{13C,bveg}F_{gpp,land} - f_{13C,veg}(F_{res,land} + F_{turnover}) \\ \frac{d}{dt}(^{13}C_{soil}) =& f_{13C,veg}F_{turnover} - f_{13C,soil}F_{htr,land} - f_{13C,soil}F_{bg,land},\end{aligned} \quad (21)$$

where f_{13C} is the fraction of ^{13}C to total *C* in each reservoir ($f_{13C} = {}^{13}C/({}^{12}C + {}^{13}C)$); and $F_{ao,\uparrow}$ and $F_{ao,\downarrow}$ are the upward and downward counterparts of F_{ao}, respectively. The estimated amount of ^{13}C is converted to carbon isotope fractionation ($\delta^{13}C$), as follows:

$$\delta^{13}C = \frac{\left(\frac{^{13}C}{^{12}C}\right)}{f_{std}} - 1, \quad (22)$$

where f_{std} is the reference value of the abundance of ^{13}C relative to ^{12}C (f_{std} = 0.0112372).

The *C* isotope fractionation occurs when CO_2 exchanges at the air-sea interface, when land or marine ecosystems assimilate carbon, and when $CaCO_3$ is formed and removed from the ocean ($\Delta\delta^{13}C_{pc}$ = 1.2‰). We considered the temperature-dependent isotope *C* fractionation, as follows[68,69]:

$$\Delta(\delta^{13}C_{pc}) = 1.2(‰) \quad (23)$$

$$\Delta(\delta^{13}C_{oa}) = 10.6 - 0.1(T_s - 273.15)(‰) \quad (24)$$

$$\Delta(\delta^{13}C_{ao}) = 1.6.(‰) \quad (25)$$

The *C* isotope fractionation owing to the *C* assimilation by land and marine biosphere is represented as follows[70,71]:

$$\Delta(\delta^{13}C_{org,land}) = a_{land}\left(1 - \frac{p_i}{p_a}\right) + b_{land}\frac{p_i}{p_a} \quad (26)$$

$$\begin{aligned}\Delta(\delta^{13}C_{org,marine}) =& 11.98 - 0.12(T_s - 273.15) + (25 - (159.5 * [PO_4^{3-}]_{surf}(\mu M) \\ &+ 38.39)/([H_2CO_3]_{surf}(\mu M)), (‰)\end{aligned} \quad (27-28)$$

where a_{land} is the fractionation of *C* due to diffusion of air (a_{land} = 4.4‰)[72], b_{land} is the net *C* fractionation by carboxylation (b_{land} = 27‰)[73], and p_a and p_i are the ambient and intercellular pCO_2, respectively. The p_i/p_a ratio changes in accordance with the opening of the plant's stomata, and it tends to be kept relatively constant in present environments, reflecting the adjustment of the stomatal conductance by plants to maintain their optimal condition[74,75]. It has been pointed out, however, that p_i/p_a ratio would depend on many factors such as temperature and precipitation[76]. In addition, when the atmospheric pCO_2 is especially high, it may approach unity owing to the upper limit of the stomatal resistance, assuming the breakdown of the optimal stomatal behavior[77]. Because our focus here is the responses during the periods of high atmospheric pCO_2 after the Ontong Java Nui eruption, we adopted a value of p_i/p_a ratio of unity.

Experiment setup. Using this model, we estimated the steady state of the global carbon and phosphorus cycles before the eruption of Ontong Java Nui by running the model without forcing the CO_2 influx supplied by the eruption. We fixed the boundary conditions of the model (e.g., solar luminosity, land area, etc.) to the condition assuming 120 Ma. The CO_2 emission from the eruption of the Ontong Java Nui is given to the model from 119.3 Ma, starting from the steady state obtained for the 120 Ma condition. We conducted a series of experiments with different values of the total CO_2 emission and the period of the CO_2 emission. We run the model with different total CO_2 emissions for a sustained period of 400 kyr (Supplementary Fig. 7a). The total CO_2 emission is varied from 0 to 100 % of the maximum value estimated from the mass of the Ontong Java Plateau (1.0×10^{21} g CO_2; ~2.7×10^5 GtC)[42], which is given to the model at a constant supply rate. We also run the model with different periods of the eruption of the CO_2 emission with the total CO_2 emission of 70 % of the maximum value[42]. The duration of the CO_2 emission is changed from 100 to 1000 kyr at each 100 kyr (Supplementary Fig. 7b).

Calculation of Os fluxes using a simple box model

The changes in the Os flux from the OJN volcanism were calculated by a simple box model of ref. [4]. This model assumes the ocean as a unique Os reservoir, and Os amount and isotopic composition of seawater reflect the balance between continental input, hydrothermal input related to oceanic crust, volcanic input from OJN, extraterrestrial input, and a sedimentary

sink. These relationships are described as:

$$\frac{dM_{ocean}}{dt} = F_{cont} + F_{hydr} + F_{cosm} + F_{OJN} - F_{sed} \quad (29)$$

$$\frac{d(M_{ocean}R_{ocean})}{dt} = F_{cont}R_{cont} + F_{hydr}R_{hydr} + F_{cosm}R_{cosm} + F_{OJN}R_{OJN} - F_{sed}R_{sed} \quad (30)$$

where M, F, and R represent the amount, flux, and Os isotopic ratio ($^{187}Os/^{188}Os$), and the subscripts 'ocean', 'cont', 'hydr', 'cosm', 'OJN', and 'sed' represent the oceanic reservoir, riverine input, hydrothermal input, extraterrestrial input, input from the OJN, and sedimentary output, respectively. We assume that R_{sed} coincides with R_{ocean}. The above equations can be transformed as:

$$\frac{dR_{ocean}}{dt} = \frac{[F_{cont}(R_{cont} - R_{ocean}) + F_{hydr}(R_{hydr} - R_{ocean}) + F_{cosm}(R_{cosm} - R_{ocean}) + F_{OJN}(R_{OJN} - R_{ocean})]}{M_{ocean}} \quad (31)$$

Here, we used the present-day values of F_{cont} = 295 t/kyr, R_{cont} = 1.54, R_{hydr} = 0.126, F_{cosm} = 17.6 t/kyr, and R_{cosm} = 0.126 for the background conditions before OAE1a[78]. In the steady background condition, we set F_{hydr} = 567.4 t/kyr to match the background seawater Os isotopic values (R_{ocean} = 0.6). We assumed that F_{sed} varies proportionally to M_{ocean}, and set the coefficient of proportionality at 0.056 following ref. [4]. We set the Os isotopic composition of OJN as $^{187}Os/^{188}Os$ = 0.146 changed the F_{OJN} to match the observed Os isotopic data[4].

Data availability

The data supporting our new findings are available within the Supplementary Tables of this article.

Code availability

The source code of the biogeochemical box model and marine osmium model can be obtained from the corresponding author upon request.

Received: 1 August 2023; Accepted: 7 March 2024;
Published online: 26 March 2024

References

1. Chandler, M. T. et al. Reconstructing Ontong Java Nui: implications for Pacific absolute plate motion, hotspot drift and true polar wander. *Earth Planet. Sci. Lett.* **331**, 140–151 (2012).
2. Taylor, B. The single largest oceanic plateau: Ontong Java–Manihiki–Hikurangi. *Earth Planet. Sci. Lett.* **241**, 372–380 (2006).
3. Petterson, M. G. et al. Structure and deformation of north and central Malaita, Solomon Islands: tectonic implications for the Ontong Java Plateau-Solomon arc collision, and for the fate of oceanic plateaus. *Tectonophysics* **283**, 1–33 (1997).
4. Tejada, M. L. G. et al. Ontong Java Plateau eruption as a trigger for the early Aptian oceanic anoxic event. *Geology* **37**, 855–858 (2009).
5. Erba, E. et al. Environmental consequences of Ontong Java Plateau and Kerguelen plateau volcanism. *In:* The origin, evolution, and environmental impact of oceanic large igneous provinces. (eds. Neal, C. R., Sager, W. W., Sano, T., and Erba, E.) *Geol. Soc. Am. Spec. Pap*. **511**, 271–303 (2015).
6. Olierook, H. K., Jourdan, F. & Merle, R. E. Age of the Barremian–Aptian boundary and onset of the Cretaceous normal superchron. *Earth-Sci. Rev.* **197**, 102906 (2019).
7. Larson, R. L. & Erba, E. Onset of the Mid-Cretaceous greenhouse in the Barremian-Aptian: igneous events and the biological, sedimentary, and geochemical responses. *Paleoceanography* **14**, 663–678 (1999).
8. Sikora, P. J. & Bergen, J. A. Lower Cretaceous planktonic foraminiferal and nannofossil biostratigraphy of Ontong Java Plateau sites from DSDP Leg 30 and ODP Leg 192. *In:* Origin and evolution of the Ontong Java Plateau. (eds. Fitton, J. G., Mahoney, J. J., Wallace, P. J., & Saunders, A. D.) *Geol. Soc. London Spec. Publ*. **229**, 83–111 (2004).
9. Davidson, P. C., Koppers, A. A. P., Sano, T. & Hanyu, T. A younger and protracted emplacement of the Ontong Java Plateau. *Science* **380**, 1185–1188 (2023).
10. Kuroda, J. et al. Lead isotopic record of Barremian–Aptian marine sediments: Implications for large igneous provinces and the Aptian climatic crisis. *Earth Planet. Sci. Lett.* **307**, 126–134 (2011).
11. Bottini, C., Cohen, A. S., Erba, E., Jenkyns, H. C. & Coe, A. L. Osmium-isotope evidence for volcanism, weathering, and ocean mixing during the early Aptian OAE 1a. *Geology* **40**, 583–586 (2012).
12. Price, G. D. New constraints upon isotope variation during the early Cretaceous (Barremian–Cenomanian) from the Pacific Ocean. *Geol. Mag.* **140**, 513–522 (2003).
13. Ando, A., Kaiho, K., Kawahata, H. & Kakegawa, T. Timing and magnitude of early Aptian extreme warming: Unraveling primary $\delta^{18}O$ variation in indurated pelagic carbonates at deep sea drilling project site 463, central Pacific Ocean. *Palaeogeogr. Palaeoclimatol. Palaeoecol.* **260**, 463–476 (2008).
14. Tarduno, J. A. et al. Rapid formation of Ontong Java Plateau by Aptian mantle plume volcanism. *Science* **254**, 399–403 (1991).
15. Sliter, W. V. Cretaceous planktic foraminiferal biostratigraphy of the Calera Limestone, northern California, USA. *J. Foraminifer. Res.* **29**, 318–339 (1999).
16. Thiede, J. et al. Site 463: western mid-Pacific mountains. *In*: Initial reports of the deep sea drilling project (eds. Thiede, J., Vallier, T. L., Adelseck, C. G. et al.) **62**, 33–156 (1981).
17. Ando, A. Intersite discrepancy in the amplitude of marine negative ^{13}C excursion at the onset of early Aptian oceanic anoxic event 1a: Reconciliation through Sr isotopic screening of peculiar diagenetic overprint on the Pacific reference section (Deep Sea Drilling Project Site 463). *In*: The origin, evolution, and environmental impact of oceanic large igneous provinces. (eds. Neal, C. R., Sager, W. W., Sano, T., and Erba, E.) *Geol. Soc. Am. Spec. Pap*. **511**, 329 (2015).
18. Li, Y. X. et al. Toward an orbital chronology for the early Aptian oceanic anoxic event (OAE1a,~ 120 Ma). *Earth Planet. Sci. Lett.* **271**, 88–100 (2008).
19. Matsumoto, H. et al. Marine Os isotopic evidence for multiple volcanic episodes during cretaceous oceanic anoxic event 1b. *Sci. Rep.* **10**, 12601 (2020).
20. Matsumoto, H. et al. Long-term Aptian marine osmium isotopic record of Ontong Java Nui activity. *Geology* **49**, 1148–1152 (2021).
21. Khondoker, R. et al. New constraints on elemental and Pb and Nd isotope compositions of South American and Southern African aerosol sources to the South Atlantic Ocean. *Geochem* **78**, 372–384 (2018).
22. Schleicher, N. J. et al. A global assessment of copper, zinc, and lead isotopes in mineral dust sources and aerosols. *Front. Earth Sci.* **8**, 167 (2020).
23. Castillo, P. R. Geochemistry of Cretaceous volcaniclastic sediments in the Nauru and East Mariana basins provides insights into the mantle sources of giant oceanic plateaus. in *Origin and Evolution of the Ontong Java Plateau*. (eds. Fitton, J. G., Mahoney, J. J., Wallace, P. J., Saunders, A. D.) *Geol. Soc. Spec. Publ*. **229**, 353–368 (2004).
24. Shafer, J. T., Neal, C. R. & Castillo, P. R. Compositional variability in lavas from the Ontong Java Plateau: Results from basalt clasts within the volcaniclastic succession at Ocean Drilling Program site 1184. in *Origin and Evolution of the Ontong Java Plateau*. (eds. Fitton, J. G.,

Mahoney, J. J., Wallace, P. J., Saunders, A. D.) *Geol. Soc. London Spec. Publ*. **229**, 333–351 (2004).
25. White, R. V., Castillo, P. R., Neal, C. R., Fitton, J. G. & Godard, M. Phreatomagmatic eruptions on the Ontong Java Plateau: chemical and isotopic relationship to Ontong Java Plateau basalts. in *Origin and Evolution of the Ontong Java Plateau*. (eds. Fitton, J. G., Mahoney, J. J., Wallace, P. J., Saunders, A. D.) *Geol. Soc. London Spec. Publ*. **229**, 307–323 (2004).
26. Ling, H. F. et al. Differing controls over the Cenozoic Pb and Nd isotope evolution of deepwater in the central North Pacific Ocean. *Earth Planet. Sci. Lett.* **232**, 345–361 (2005).
27. Konter, J. G. et al. One hundred million years of mantle geochemical history suggest the retiring of mantle plumes is premature. *Earth Planet. Sci. Lett.* **275**, 285–295 (2008).
28. Thordarson, T. Accretionary-lapilli-bearing pyroclastic rocks at ODP Leg 192 Site 1184: a record of subaerial phreatomagmatic eruptions on the Ontong Java Plateau. in *Origin and Evolution of the Ontong Java Plateau*. (eds. Fitton, J. G., Mahoney, J. J., Wallace, P. J. & Saunders, A. D.) *Geol. Soc. London Spec. Publ*. **229**, 275–306 (2004).
29. Timm, C. et al. Age and geochemistry of the oceanic Manihiki Plateau, SW Pacific: New evidence for a plume origin. *Earth Planet. Sci. Lett.* **304**, 135–146 (2011).
30. Ai, H. A., Stock, J. M., Clayton, R. & Luyendyk, B. Vertical tectonics of the High Plateau region, Manihiki Plateau, Western Pacific, from seismic stratigraphy. *Mar. Geophys. Res.* **29**, 13–26 (2008).
31. Roberge, J., Wallace, P. J., White, R. V. & Coffin, M. F. Anomalous uplift and subsidence of the Ontong Java Plateau inferred from CO_2 contents of submarine basaltic glasses. *Geology* **33**, 501–504 (2005).
32. Egger, H. & Brückl, E. Gigantic volcanic eruptions and climatic change in the early Eocene. *Int. J. Earth Sci.* **95**, 1065–1070 (2006).
33. Tejada, M. L. G., Mahoney, J. J., Neal, C. R., Duncan, R. A. & Petterson, M. G. Basement geochemistry and geochronology of Central Malaita, Solomon Islands, with implications for the origin and evolution of the Ontong Java Plateau. *J. Petrol.* **43**, 449–484 (2002).
34. Hoernle, K. et al. Age and geochemistry of volcanic rocks from the Hikurangi and Manihiki oceanic Plateaus. *Geochim. Cosmochim. Acta* **74**, 7196–7219 (2010).
35. Golowin, R. et al. Geochemistry of deep Manihiki Plateau crust: implications for compositional diversity of large igneous provinces in the Western Pacific and their genetic link. *Chem. Geol.* **493**, 553–566 (2018).
36. Koppers, A. A., Staudigel, H., Pringle, M. S., & Wijbrans, J. R. Short-lived and discontinuous intraplate volcanism in the South Pacific: hot spots or extensional volcanism? *Geochem. Geophys. Geosyst*. **4** 1089 (2003).
37. Shimoda, G. et al. Tectonic influence on chemical composition of ocean island basalts in the West and South Pacific: Implication for a deep mantle origin. *Geochem. Geophys. Geosyst.* **12**, Q07020 (2011).
38. Yamaoka, K. & Wallis, S. R. Clockwise rotation of SW Japan and timing of Izanagi–Pacific ridge subduction revealed by arc migration. *Prog. Earth Planet. Sci.* **10**, 62 (2023).
39. Takagi, T. Origin of magnetite-and ilmenite-series granitic rocks in the Japan arc. *Am. J. Sci.* **304**, 169–202 (2004).
40. Ji, Z. et al. Early Cretaceous adakitic lavas and A-type rhyolites in the Songliao Basin, NE China: Implications for the mechanism of lithospheric extension. *Gondwana Res.* **71**, 28–48 (2019).
41. Gales, E., Black, B. & Elkins-Tanton, L. T. Carbonatites as a record of the carbon isotope composition of large igneous province outgassing. *Earth Planet. Sci. Lett.* **535**, 116076 (2020).
42. Roberge, J., White, R. V. & Wallace, P. J. Volatiles in submarine basaltic glasses from the Ontong Java Plateau (ODP Leg 192): implications for magmatic processes and source region compositions. *In:* Origin and evolution of the Ontong Java Plateau. (eds. Fitton, J. G., Mahoney, J. J., Wallace, P. J., & Saunders, A. D.) *Geol. Soc. London Spec. Publ*. **229**, 239–257 (2004).
43. Bauer, K. W., Zeebe, R. E. & Wortmann, U. G. Quantifying the volcanic emissions which triggered Oceanic Anoxic Event 1a and their effect on ocean acidification. *Sedimentology* **64**, 204–214 (2017).
44. Sharma, M., Balakrishna, K., Hofmann, A. W. & Shankar, R. The transport of osmium and strontium isotopes through a tropical estuary. *Geochim. Cosmochim. Acta* **71**, 4856–4867 (2007).
45. Tejada, M. L. G. et al. Cryptic lower crustal signature in the source of the Ontong Java Plateau revealed by Os and Hf isotopes. *Earth Planet. Sci. Lett.* **377**, 84–96 (2013).
46. Matsumoto, H. et al. Mid-Cretaceous marine Os isotope evidence for heterogeneous cause of oceanic anoxic events. *Nat. Commun.* **13**, 239 (2022).
47. Ishikawa, A., Pearson, D. G. & Dale, C. W. Ancient Os isotope signatures from the Ontong Java Plateau lithosphere: Tracing lithospheric accretion history. *Earth Planet. Sci. Lett.* **301**, 159–170 (2011).
48. Sano, T. Homogenization of magmas from the Ontong Java Plateau: Olivine-spinel compositional evidence. *In:* The origin, evolution, and environmental impact of oceanic large igneous provinces. (eds. Neal, C. R., Sager, W. W., Sano, T., and Erba, E.) *Spec. Pub. Geol. Soc. Am*. **511**, 221–232 (2015).
49. Castro, J. M. et al. High-resolution C-isotope, TOC and biostratigraphic records of OAE 1a (Aptian) from an expanded hemipelagic cored succession, western Tethys: a new stratigraphic reference for global correlation and paleoenvironmental reconstruction. *Paleoceanogr. Paleoclimatol.* **36**, e2020PA004004 (2021).
50. Bottini, C. et al. Climate variability and ocean fertility during the Aptian stage. *Clim. Past* **11**, 383–402 (2015).
51. Shirey, S. B. & Walker, R. J. Carius tube digestion for low-blank rhenium-osmium analysis. *Anal. Chem.* **67**, 2136–2141 (1995).
52. Cohen, A. S. & Waters, F. G. Separation of osmium from geological materials by solvent extraction for analysis by thermal ionisation mass spectrometry. *Anal. Chim. Acta* **332**, 269–275 (1996).
53. Pearson, D. G. & Woodland, S. J. Solvent extraction/anion exchange separation and determination of PGEs (Os, Ir, Pt, Pd, Ru) and Re–Os isotopes in geological samples by isotope dilution ICP-MS. *Chem. Geol.* **165**, 87–107 (2000).
54. Birck, J. L., Barman, M. R. & Capmas, F. Re-Os isotopic measurements at the femtomole level in natural samples. *Geostand. Newsl.* **21**, 19–27 (1997).
55. Smoliar, M. I., Walker, R. J. & Morgan, J. W. Re-Os ages of group IIA, IIIA, IVA, and IVB iron meteorites. *Science* **271**, 1099–1102 (1996).
56. Goto, K. T. et al. Paleoceanographic conditions on the São Paulo Ridge, SW Atlantic Ocean, for the past 30 million years inferred from Os and Pb isotopes of a hydrogenous ferromanganese crust. *Deep-Sea Res. II: Top. Stud. Oceanogr.* **146**, 82–92 (2017).
57. Taylor, R. N., Ishizuka, O., Michalik, A., Milton, J. A. & Croudace, I. W. Evaluating the precision of Pb isotope measurement by mass spectrometry. *J. Anal. At. Spectrom.* **30**, 198–213 (2015).
58. Baker, J., Peate, D., Waight, T. & Meyzen, C. Pb isotopic analysis of standards and samples using a 207Pb–204Pb double spike and thallium to correct for mass bias with a double-focusing MC-ICP-MS. *Chem. Geol.* **211**, 275–303 (2004).
59. Jochum, K. P. et al. Reference values following ISO guidelines for frequently requested rock reference materials. *Geostand. Geoanal. Res.* **40**, 333–350 (2016).
60. Ozaki, K. & Reinhard, C. T. The future lifespan of Earth's oxygenated atmosphere. *Nat. Geosci.* **14**, 138–142 (2021).
61. Williams, D. M. & Kasting, J. F. Habitable planets with high obliquities. *Icarus* **129**, 254–267 (1997).

62. Caldeira, K. & Kasting, J. F. The life span of the biosphere revisited. *Nature* **360**, 721–723 (1992).
63. Lenton, T. M., Daines, S. J. & Mills, B. J. COPSE reloaded: an improved model of biogeochemical cycling over Phanerozoic time. *Earth-Sci. Rev.* **178**, 1–28 (2018).
64. Nederbragt, A. J., Thurow, J., Vonhof, H. & Brumsack, H. J. Modelling oceanic carbon and phosphorus fluxes: implications for the cause of the late Cenomanian Oceanic Anoxic Event (OAE2). *J. Geol. Soc. London* **161**, 721–728 (2004).
65. Slomp, C. P. & Van Cappellen, P. The global marine phosphorus cycle: sensitivity to oceanic circulation. *Biogeosciences* **4**, 155–171 (2007).
66. Kraal, P., Slomp, C. P., Forster, A. & Kuypers, M. M. M. Phosphorus cycling from the margin to abyssal depths in the proto-Atlantic during oceanic anoxic event 2. *Palaeogeogr. Palaeoclimatol. Palaeoecol.* **295**, 42–54 (2010).
67. Yamanaka, Y. & Tajika, E. The role of the vertical fluxes of particulate organic matter and calcite in the oceanic carbon cycle: Studies using an ocean biogeochemical general circulation model. *Glob. Biogeochem. Cycles* **10**, 361–382 (1996).
68. Walker J. C. G. Numerical adventures with geochemical cycles. (Oxford University Press, 1990)
69. Bjerrum, C. J. & Canfield, D. E. Towards a quantitative understanding of the late Neoproterozoic carbon cycle. *Proc. Natl. Acad. Sci.* **108**, 5542–5547 (2011).
70. Farquhar, G. D., O'Leary, M. H. & Berry, J. A. On the relationship between carbon isotope discrimination and the intercellular carbon dioxide concentration in leaves. *Funct. Plant. Biol.* **9**, 121–137 (1982).
71. Kump, L. R., & Arthur, M. A. Interpreting carbon-isotope excursions: carbonates and organic matter. *Chem. Geo.*, **161**, 181–198 (1999).
72. Craig, H. Carbon 13 in plants and the relationships between carbon 13 and carbon 14 variations in nature. *J. Geol.* **62**, 115–149 (1954).
73. Farquhar, G. D. & Richards, R. A. Isotopic composition of plant carbon correlates with water-use efficiency of wheat genotypes. *Funct. Plant. Biol.* **11**, 539–552 (1984).
74. Cowan I. R. & Farquhar G. D. Stomatal function in relation to leaf metabolism and environment. *In:* Integration of activity in the higher plant. (eds. Jennings D. H.) 471–505 (Cambridge: at the university press, 1977)
75. Prentice, I. C., Dong, N., Gleason, S. M., Maire, V. & Wright, I. J. Balancing the costs of carbon gain and water transport: testing a new theoretical framework for plant functional ecology. *Ecol. Lett.* **17**, 82–91 (2014).
76. Belmecheri, S. et al. Precipitation alters the CO_2 effect on water-use efficiency of temperate forests. *Glob. Chang. Biol.* **27**, 1560–1571 (2021).
77. Keeling, R. F. et al. Atmospheric evidence for a global secular increase in carbon isotopic discrimination of land photosynthesis. *Proc. Natl. Acad. Sci.* **114**, 10361–10366 (2017).
78. Levasseur, S., Birck, J. L. & Allegre, C. J. The osmium riverine flux and the oceanic mass balance of osmium. *Earth Planet. Sci. Lett.* **174**, 7–23 (1999).
79. Mahoney, J. J., Duncan, R. A., Tejada, M. L. G., Sager, W. W. & Bralower, T. J. Jurassic-Cretaceous boundary age and mid-ocean-ridge–type mantle source for Shatsky Rise. *Geology* **33**, 185–188 (2005).
80. Heydolph, K. et al. Plume versus plate origin for the Shatsky Rise oceanic plateau (NW Pacific): Insights from Nd, Pb and Hf isotopes. *Lithos* **200**, 49–63 (2014).
81. Tejada, M. L. G. et al. Pin-pricking the elephant: Evidence on the origin of the Ontong Java Plateau from Pb-Sr-Hf-Nd isotopic characteristics of ODP Leg 192 basalts. In: Origin and evolution of the Ontong Java Plateau. (eds. Fitton, J. G., Mahoney, J. J., Wallace, P. J., & Saunders, A. D.) *Geol. Soc. London Spec. Publ*. **229**, 133–150 (2004).
82. Tejada, M. L. G. et al. New evidence for the Ontong Java Nui hypothesis. *Sci. Rep.* **13**, 8486 (2023).
83. Tejada, M. L. G.et al. Isotopic evidence for a link between the Lyra Basin and Ontong Java plateau. *In:* The origin, evolution, and environmental impact of oceanic large igneous provinces. (eds. Neal, C. R., Sager, W. W., Sano, T., & Erba, E.) *Spec. Pub. Geol. Soc. Am*. **511**, 251–269 (2015).
84. Ingle, S. et al. Depleted mantle wedge and sediment fingerprint in unusual basalts from the Manihiki Plateau, central Pacific Ocean. *Geology* **3**, 595–598 (2007).
85. Golowin, R. et al. The role and conditions of second-stage mantle melting in the generation of low-Ti tholeiites and boninites: the case of the Manihiki Plateau and the Troodos ophiolite. *Contrib. Mineral. Petrol.* **172**, 1–18 (2017).
86. Tejada, M. L. G. et al. Geochemistry and age of Shatsky, Hess, and Ojin rise seamounts: implications for a connection between the shatsky and hess rises. *Geochim. Cosmochim. Acta* **185**, 302–327 (2016).
87. Ferrat, M. et al. Lead atmospheric deposition rates and isotopic trends in Asian dust during the last 9.5 kyr recorded in an ombrotrophic peat bog on the eastern Qinghai–Tibetan plateau. *Geochim. Cosmochim. Acta* **82**, 4–22 (2012).

Acknowledgements

We thank Y. Otsuki and J. Kikuchi for their support in the Re-Os analysis. We are deeply indebted to K. Tanaka and N. Izumoto for their help in the $\delta^{13}C_{carb}$ analysis. We also thank K. Ozaki and E. Tajika for supporting the construction of the biogeochemical box model. This study was financially supported by a Grant-in-aid for a Japan Society for the Promotion of Science Research Fellow (19J20708 and 22J00271). This manuscript was highly improved by the comments and suggestions of professor Loÿc Vanderkluysen and two anonymous reviewers. Samples were provided by the International Ocean Discovery Program (IODP) (Sample request numbers 071305IODP, 073623IODP, 075591IODP, 089443IODP, and 092296IODP).

Author contributions

H.M., J.K., A.I. and M.L.G.T performed Re-Os analysis. H.M., K.T.G. and G.S. performed Pb isotope analysis. H.M. and K.S. performed carbon isotopic analysis. Y.W. performed global C and P cycle modeling. H.M. performed Os cycle modeling. H.M. performed micropaleontological observations. The original manuscript was written by H.M. K.T.G., G.S., Y.W., K.S., M.L.G.T., A.I., A.A., T.S., J.K. and K.S. contributed to the discussion and provided comments on the manuscript.

Competing interests

We declare no competing interests.

Additional information

Supplementary information The online version contains supplementary material available at https://doi.org/10.1038/s43247-024-01310-0.

Correspondence and requests for materials should be addressed to Hironao Matsumoto.

Peer review information *Communications Earth & Environment* thanks Jerzy Blusztajn, Ingrid Ukstins-Peate and Loÿc Vanderkluysen for their contribution to the peer review of this work. Primary Handling Editors: Xiaoming Liu and Joe Aslin. A peer review file is available.